Applied Physics Letters

Defects controlled doping and electrical transport in TiS_2 single crystals

Cite as: Appl. Phys. Lett. **116**, 121901 (2020); https://doi.org/10.1063/5.0005170
Submitted: 18 February 2020 . Accepted: 11 March 2020 . Published Online: 24 March 2020

Ke Chen, Meng Song, Yi-Yang Sun, Hai Xu, Dong-Chen Qi, Zhenhuang Su, Xingyu Gao, Qian Xu, Jun Hu, Junfa Zhu, Ranran Zhang, Jie Wang, Lei Zhang, Liang Cao, Yuyan Han, and Yimin Xiong

Applied Physics Letters ARTICLE scitation.org/journal/apl

Defects controlled doping and electrical transport in TiS_2 single crystals

Cite as: Appl. Phys. Lett. **116**, 121901 (2020); doi: 10.1063/5.0005170
Submitted: 18 February 2020 · Accepted: 11 March 2020 ·
Published Online: 24 March 2020

Ke Chen,[1,2] Meng Song,[1,2] Yi-Yang Sun,[3] Hai Xu,[4,5] Dong-Chen Qi,[6,7] Zhenhuang Su,[8] Xingyu Gao,[8] Qian Xu,[9] Jun Hu,[9] Junfa Zhu,[9] Ranran Zhang,[1] Jie Wang,[1,2] Lei Zhang,[1] Liang Cao,[1,a)] Yuyan Han,[1,a)] and Yimin Xiong[1,a)]

AFFILIATIONS

[1]Anhui Province Key Laboratory of Condensed Matter Physics at Extreme Conditions, High Magnetic Field Laboratory, Chinese Academy of Sciences, Hefei, Anhui 230031, China
[2]University of Science and Technology of China, Hefei, Anhui 230026, China
[3]State Key Laboratory of High Performance Ceramics and Superfine Microstructure, Shanghai Institute of Ceramics, Chinese Academy of Sciences, Shanghai 201899, China
[4]Changchun Institute of Optics, Fine Mechanics and Physics, Chinese Academy of Sciences, Changchun, Jilin 130033, China
[5]Center of Materials Science and Optoelectronics Engineering, University of Chinese Academy of Sciences, Beijing 100049, China
[6]Centre for Materials Science, Queensland University of Technology, Brisbane, Queensland 4001, Australia
[7]School of Chemistry and Physics, Queensland University of Technology, Brisbane, Queensland 4001, Australia
[8]Shanghai Synchrotron Radiation Facility (SSRF), Zhangjiang Laboratory, Shanghai Advanced Research Institute, Chinese Academy of Sciences, 239 Zhangheng Road, Shanghai 201204, China
[9]National Synchrotron Radiation Laboratory, University of Science and Technology of China, Hefei 230026, China

[a)]**Authors to whom correspondence should be addressed:** lcao@hmfl.ac.cn, yyhan@hmfl.ac.cn, and yxiong@hmfl.ac.cn

ABSTRACT

TiS_2 has been intensively studied as an electrode material and a thermoelectric material for energy storage and conversion applications due to its high electrical conductivity. Understanding the influence of defects on electrical transport is of importance not only to resolve the long-standing question concerning the nature of TiS_2, but also for the rational design of TiS_2 based devices for energy scavenging applications. In this study, we integrate photoemission spectroscopy, Raman spectroscopy, and electrical transport measurements to determine the chemical compositions dominated by defects and their influence on the doping and electrical properties. Our results demonstrate that TiS_2 is a heavily self-doped semiconductor with the Fermi level close to the conduction band, which serves as the conclusive experimental evidence regarding the semiconducting nature of TiS_2. The doping effect is sensitive to the (subtle) changes in the chemical composition. The electron donation from the Ti interstitials (Ti_i) to the TiS_2 host explains the high carrier concentration. The Ti Frenkel pair (Ti_F) acting as the acceptor is responsible for the decrease in the electron carrier concentration and electrical conductivity. High conductivity maintains upon partial oxidization, indicating the oxidization-tolerance in terms of the electronic structure. Our results provide valuable insight into the evolution of electronic properties modulated by defects that reveal unambiguously the self-doped semiconducting nature of TiS_2 and chemical- and environment-tolerance of TiS_2 as an advanced energy scavenging material.

TiS_2 has received considerable attention due to its potential energy scavenging application in alkali-metal ion batteries and supercapacitors serving as an intercalation host,[1–5] thermoelectric material,[6,7] and electrocatalyst,[8,9] owing to its high electrical conductivity,[10] combined with high energy density,[4] superior rate capability,[11] outstanding power factor,[12] and high catalytic activity.[13] Recently, tremendous effort has been devoted to investigating the evolution of electrical conductivity as a result of doping,[10,14,15] strain,[16] and ion intercalation,[17] in order to understand the mechanisms of charge/discharge for batteries, and the thermoelectric effect.[4,18,19] However, the nature of TiS_2 itself, either being a semimetal or semiconductor,[20,21] is still under debate.[22–26] As a consequence, it is critical to form an understanding of the fundamental properties of TiS_2 for the rational design of high performance TiS_2-based devices for energy application.

TiS_2 is one of the van der Waals (vdW) layered transition metal dichalcogenides (TMCDs) with one Ti-atom layer sandwiched between two S-atoms layers. Experimental and theoretical results reveal that the physical properties, in particular the electrical properties, are sensitive to electron-doping from defects and intercalation without structural disintegration.[7,22] This remarkable feature, on one hand, makes TiS_2 one of the most promising candidates for stable energy storage materials. On the other hand, Ti self-intercalation also complicates the electrical and thermoelectric behaviors of TiS_2, giving rise to the discrepancies regarding the nature of TiS_2. It is thus of great importance to understand the role of various types of defects in determining the electrical transport properties of TiS_2. Figure 1 shows the crystal structure of 1*T*-TiS_2 along with possible defects reported in the literature studies.[10,23] The well-known Ti interstitials (Ti_i) occupy the octahedral sites in the vdW gap between vertically stacked TiS_2 trilayers due to the low formation energy as predicted theoretically.[23] Although Ti_i has been identified as a dominant donor defect as revealed by our recent theoretical calculation,[23] the origin of the high electron concentration in TiS_2 remains controversial due to the lack of conclusive experimental evidence. In addition, the discrepancy of Ti_i contents determined from transport and thermoelectric properties indicates that other defects,[27] such as the Ti Frenkel pair (Ti_F) and oxidation, could also be responsible for producing electron carriers. For instance, oxidation by filling up the S vacancy sites could occur in TiS_2 during the material synthesis and post-treatment process, air exposure, and/or liquid phase exfoliation.[28] However, its influence on electrical transport, and in turn on the charge/discharge performance of the battery is ignored with the reasons remaining unknown.[15,28]

In this work, we aim to address the question of how electrical transport is influenced by the defects of TiS_2 and how significant can the carrier concentration and electrical conductivity be affected? This question is truly intriguing toward exploring the nature of TiS_2 and clarifying the robust intercalation-tolerance required for energy scavenging including energy conversion, storage, and catalysis. A series of defective TiS_2 single crystals were collected and characterized by a combination of photoemission spectroscopy (PES) and Raman spectroscopy. Electrical transport measurements were carried out to present the evolution of electronic properties as a function of temperature. A low temperature resistivity upturn behavior typical for doped semiconductors serves as experimental evidence to resolve the long-standing question concerning the nature of TiS_2. We have identified three types of defects and elucidated the roles they played in determining doping and electrical transport.

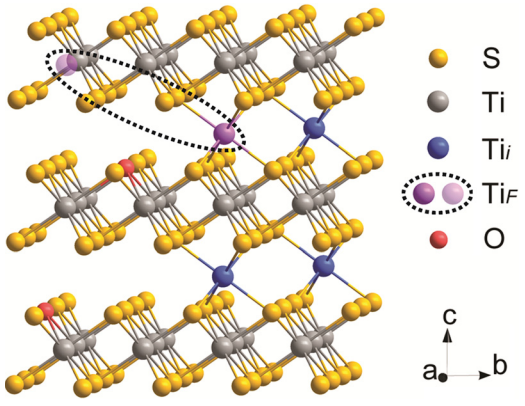

FIG. 1. Schematic illustration of the crystal structure of 1*T*-TiS_2 and the corresponding defects. The orange, gray, red, and blue balls represent the S-atoms, Ti-atoms, O-atoms, and Ti_i in the vdW gap, respectively. Ti_F (a vacancy, and an interstitial Ti in vdW gap) is depicted in purple atoms.

Three defective TiS_2 single crystals were synthesized with the details shown in the supplementary material. A single crystal was purchased from HQ Graphene for comparison purposes. To quantify the chemical composition and binding environment of the four studied samples, Ti $2p_{3/2}$ and S 2*p* core-level PES spectra were collected at room temperature (RT) and shown in Figs. 2(a) and 2(b), respectively, accompanied by the corresponding fitting curves with the parameters summarized in Tables S1 and S2 in the supplementary material. The dominant Ti $2p_{3/2}$ peak at ~456.2 eV [cf. Fig. 2(a)] is attributed to regular Ti^{4+} ions. The dominant S $2p_{3/2}$ peak is centered at ~160.8 eV [cf. Fig. 2(b)]. Both agree well with the reported PES spectra of TiS_2.[28] For the oxidized sample, a higher binding energy (BE) peak (~459.0 eV) with the position corresponding well with that of Ti^{4+} in oxides, such as TiO_2,[28,29] is attributed to the Ti–O species (cf. Fig. 1). To rule out its origin of air exposure, Ti 2*p* spectra were also measured at 600 eV with enhanced surface sensitivity to explore its distribution (surface vs bulk, cf. Fig. S2 in the supplementary material). The lower spectral weight for Ti–O species was obtained, suggesting that they are not distributed on the surface, but formed during the sample synthesis process.

In addition to the dominant features corresponding to 1*T*-TiS_2, new peaks at the lower BE side (components filled with gray) appear in both Ti $2p_{3/2}$ and S 2*p* spectra with ~1.0 and ~0.2 eV difference,

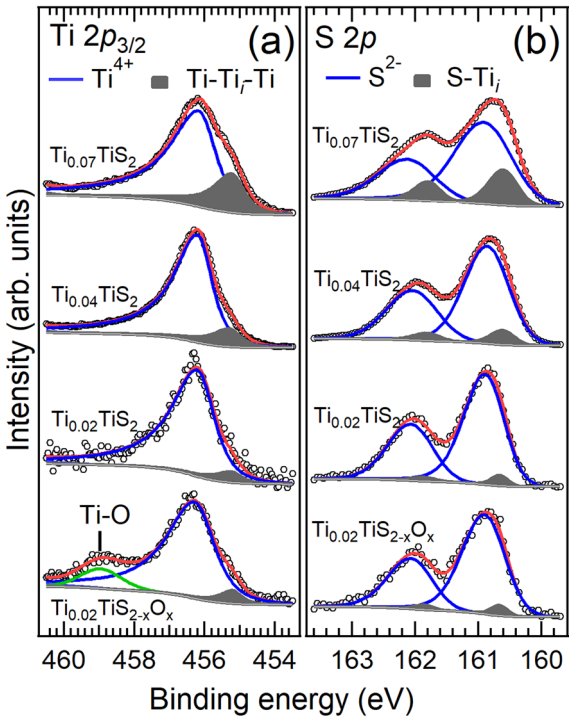

FIG. 2. (a) Ti $2p_{3/2}$ and (b) S 2*p* core-level PES spectra measured using Al K_α (1486.6 eV). The $Ti_{0.02}TiS_2$ sample was purchased from HQ Graphene.

respectively. The lower BE peak is also observed for alkali-metal-intercalated TiS_2 due to the presence of the interstitial alkali-metal.[11,13] This indicates its origin of Ti_i defects in the vdW gap with weakly S–Ti_i–S bonds (cf. Fig.1) rather than S-vacancies associated Ti^{3+} components.[30] Otherwise, no new feature is expected to be observed in the S 2*p* spectra. The charge redistribution due to the formation of Ti–S–Ti_i–S–Ti bonds (cf. Fig.1) leads to electron transfer from the Ti_i-atoms to the conduction band (CB) of the TiS_2 host, which explains the lower BE nature of new components than that of dominant peaks. It is worth noting that the lower BE features were reported before, but not well distinguished,[31] possibly due to lower defect concentration and poorer energy resolution.

The experimental Ti:S ratio estimated from the intensity of Ti $2p_{3/2}$ and S $2p_{3/2}$ core-levels (cf. Table S3 in the supplementary material) normalized with respect to average matrix relative sensitivity factors is close to a stoichiometric ratio of 1:2 for all samples,[32] which is in line with the energy dispersive x-ray spectroscopy (EDX) results (cf. Table S3 in the supplementary material). Although the defects have a negligible influence on the crystal structure of TiS_2 as revealed by the x-ray diffraction (XRD) pattern (cf. Fig. S1 in the supplementary material), the appearance of new components in the PES spectra indicates the existence of a significant amount of defects. The spectra weight due to Ti_i is expected to be 1/3 for the Ti–S–Ti_i–S–Ti species. As a consequence, the nominal Ti_i contents δ of 0.07, 0.04, 0.02, for $Ti_\delta TiS_2$, and 0.02 for the oxidized sample are determined from the intensity ratio of 1/3∗Ti-Ti_i-Ti/(Ti^{4+}+2/3∗Ti-Ti_i-Ti)(cf. Table S1 in the supplementary material) and shown in the molecular formula in Fig.2. The intensity ratio of Ti–Ti_i–Ti/S–Ti_i of 2.24:4 for $Ti_{0.07}TiS_2$ is lower than that of ∼3:4 for the other three samples (cf. Table S3 in the supplementary material), implying the coexistence of Ti-vacancies and interstitial Ti and thus the presence of Ti_F (cf. Fig. 1).

Raman spectroscopy was conducted to investigate the effect of chemical composition on the vibration properties as shown in Fig. 3. Out-of-plane A_{1g} and in-plane E_g modes associated vibrational peaks for 1*T*-TiS_2, and the corresponding two shoulders of Sh(A_{1g}) and Sh(E_g) are located at ∼332, ∼230, ∼380, and ∼205 cm^{-1}, respectively, which are consistent with the literature.[33] Two new vibrational peaks (labeled by #) at ∼273 and ∼350 cm^{-1} are close to the modes (275 and 343 cm^{-1}) associated with TiS,[31] and are believed to originate from Ti_i defects. A stronger interaction due to chemical bonds than vdW interaction leads to the stiffening of # peaks compared to the A_{1g} and E_g modes. The blue shift of the Sh(A_{1g}) with increasing Ti_i concentration suggests that this shoulder is sensitive to interlayer coupling strength.[33] The mode for anatase TiO_2 (∼144 cm^{-1}) was not detected even for $Ti_{0.02}TiS_{2-x}O_x$,[34] ruling out the presence of the TiO_2 secondary phase.

To explore the influence of defects on the electronic properties, electrical transport measurements were performed. Figure 4(a) shows the temperature-dependent in-plane resistivity ρ_{xx}. All resistivity curves show a metallic behavior in the range of 15–300 K, which has been coined as the semimetal nature of TiS_2 as reported previously.[35,36] In general, the resistivity value increases with increasing Ti_i concentration. In contrast, the oxidized $Ti_{0.02}TiS_{2-x}O_x$ shows a distinct behavior, and displays a comparably low temperature residual resistivity (<20 K) and a much higher RT resistivity. These indicate different mechanisms dominating the transport behavior and different nature of the carriers in $Ti_{0.02}TiS_{2-x}O_x$ due to partial oxidization.

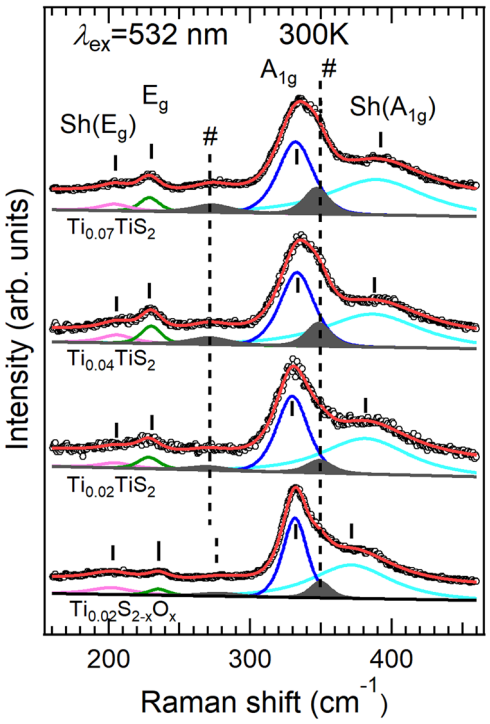

FIG. 3. Raman spectra obtained using a 532 nm laser collected at RT and the corresponding fitting peaks.

To understand the scattering mechanism and its temperature dependence, a power law fitting of $\rho(T) = \rho_0 + AT^\alpha$ was performed with the fitting results shown in Fig. S3(a) in the supplementary material. The yielded residual resistivity ρ_0, and the exponent α determined by the dominant scattering mechanism are summarized in Table I. α shows the obvious temperature and chemical composition dependences. At a low temperature of 15–50 K, α is close to 3 for three $Ti_\delta TiS_2$ samples, resulting from an interband *s*-*d* electron-phonon scattering, which is in line with the literature studies.[27,37] In contrast, a relatively low α of 2.57 is obtained for $Ti_{0.02}TiS_{2-x}O_x$ with the scattering mechanism remaining elusive. At a higher temperature of $T > 100$ K, the temperature dependence evolves into a T^2 behavior for all four samples due to a dominant electron-phonon coupling. The deviation from 2 is most likely explained by the disorder induced by Ti_i and/or Ti_F defects, which is consistent with the stiffening of Raman modes.

For three $Ti_\delta TiS_2$ samples, ρ_0 increases with increasing δ (Table I), whereas the residual resistivity ratio (RRR) decreases due to enhanced scattering arising from Ti_i as well as other potential point defects. This is consistent with the Ti_i-related features as revealed by PES and Raman measurements. In oxidized $Ti_{0.02}TiS_{2-x}O_x$, ρ_0 is slightly increased as compared to that of $Ti_{0.02}TiS_2$ and RRR is almost doubled. These results suggest that oxidation causes a subtle increase in defects, while the RRR value is mainly affected by other factors, such as carrier density and mobility.

It is notable that low-*T* resistivities of all samples exhibit an upturn behavior below 15 K as shown in Fig. 4(b), which has not been reported previously. Possible mechanisms, such as weak localization (WL) and/or Kondo effect,[38,39] can be ruled out because of the nearly

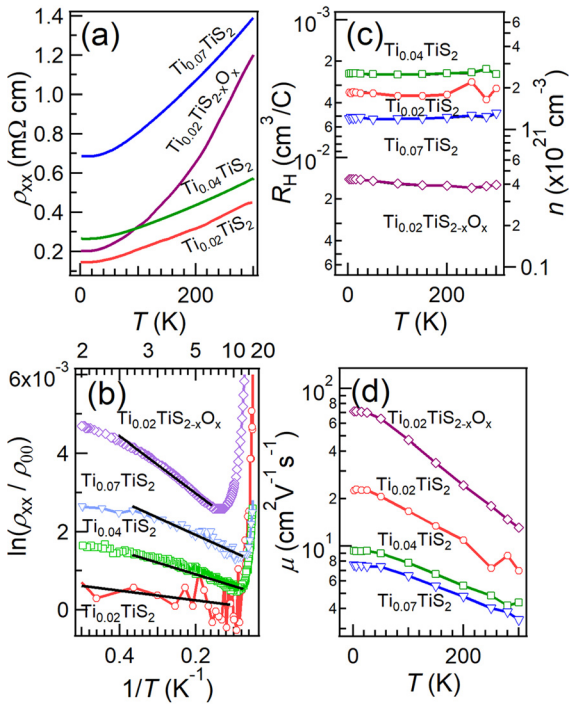

FIG. 4. (a) The temperature dependent in-plane resistivity ρ_{xx}, and (b) $\ln(\rho_{xx}/\rho_{00})$ as a function of $1/T$ with $2 \leq T \leq 20$ K. The curves in panel b are shift vertically for the sake of clarity. Temperature dependence of (c) the ordinary Hall coefficient R_H and the corresponding carrier concentrations calculated by using $n = (eR_H)^{-1}$, and (d) carrier mobility $\mu = R_H/\rho_{xy}$.

magnetic field independent resistivity up to 9 Tesla at 2 K [cf. Fig. S3(b) in the supplementary material]. As a consequence, this upturn behavior can be best explained by the semiconducting nature of bulk TiS_2. As a heavily self-doped semiconductor caused by the presence of Ti_i and Ti_F, at a low temperature (*extrinsic region*), the concentration and mobility of electron carriers in CB, which are excited from the dopant levels and determined by the degree of ionization of Ti_i defects, are proportional to temperature. In such a scenario, the resistivity (inversely proportional to conductivity) can be expressed as $\rho(T) = \rho_{00} \exp(\Delta E/2k_BT)$, in which ΔE is the energy difference between CB and donor levels, and ρ_{00} is the pre-exponential factor. ΔE determined from the fitting results [solid lines in Fig. 4(b)] is on the order of 10^{-7} eV as listed in Table I, which is consistent with our recent theoretical calculation that the Fermi level of TiS_2 is close to the CB.[23] The wide temperature range of metallic behaviors can thus be explained by the small ΔE, ruling out the semimetal nature.[35,36]

To further reveal the contribution of defects to doping, the magnetic field dependences of Hall resistivity ρ_{xy} at different temperatures in the range of 2–300 K are measured [cf. Fig. S3(c) in the supplementary material]. The negative slopes confirm that the carrier type is electron. Figures 4(c) and 4(d) display the Hall coefficient R_H and the corresponding carrier concentrations n, and mobility μ, respectively, calculated from ρ_{xy} on the basis of a single-carrier model with the parameters at RT listed in Table I. The obtained n exhibits a weak temperature dependence and is lying between the literature region of 1.1×10^{20}–3.4×10^{21} cm^{-3}.[27,40] Assuming one Ti_i donates 4 electrons to the CB, the content of Ti_i δ can be related to n following $n = 4\delta \times (1.75 \times 10^{22})$ cm^{-3}, in which 1.75×10^{22} cm^{-3} is the density of Ti-atoms in TiS_2. δ of 0.028 and 0.036 are determined for $Ti_{0.02}TiS_2$ and $Ti_{0.04}TiS_2$, respectively, which is excellent agreement with those determined from Ti 2*p* core-level spectra. This confirms that Ti_i is the dominant donor defect in $Ti_{0.02}TiS_2$ and $Ti_{0.04}TiS_2$.

The carrier concentration is expected to increase with increased Ti_i.[12,15] However, for $Ti_{0.07}TiS_2$, δ of 0.019 is significantly lower than that of 0.07 estimated from Ti 2*p* core-level spectra, implying that the population of Ti_F becomes significant, which is in line with the PES results. The acceptor nature of Ti_F leads to the decrease in n, and thus the significant discrepancy of the estimated δ.[23] As a consequence, $Ti_{0.07}TiS_2$ has a lower n and μ, corresponding to the intensively enhanced scattering and localization induced by Ti_F. In this regards, filling of Ti-vacancies will offer a new route for tuning the conductivity properties of TiS_2, which provides valuable insights into understanding the enhancement of electrical conductivity induced by intercalation, and the underlying mechanism of charge/discharge for batteries.

For $Ti_{0.02}TiS_{2-x}O_x$, the partial oxidization causes a reduction of n and electrical conductivity, and an increase in μ. The most likely scenario is that oxidization leads to a slightly increase in the bandgap of TiS_2 as revealed by the higher BE shift (~0.03 eV) of the valence band spectra for $Ti_{0.02}TiS_{2-x}O_x$ [cf. Fig. S2(c) in the supplementary material]. It is an open question that whether a tunable bandgap as predicted theoretically[26] or two distinct bandgaps, which is the case for S-doped TiO_2,[41] can be obtained for TiS_2 with increasing O-concentration, and thus deserves a further detailed investigation.

It is worth noting that RT electrical conductivity, and n vary within an order of magnitude regardless of the type of defects, which explains the highly chemical- and environmental-tolerance of TiS_2 as an advanced energy scavenging material.[1–12] The oxidation process easily takes place after oxygen or water exposure,[29] and during the liquid phase exfoliation process.[28] The presence of Ti–O species may be responsible for the pulverization of the bulk TiS_2 electrode during discharge and charge progress,[42,43] which in turn affects energy scavenging from a mechanical point of view. A detailed understanding of the influence of various defects on the charge storage properties of

TABLE I. Parameters of ρ_0 obtained from the fitting at 15–50 K, RRR = ρ(300K)/ρ_0, α, RT carrier concentrations n, RT carrier mobility μ, and ΔE extracted from the electrical transport results.

Sample	ρ_0 (mΩ cm)	RRR	α (15–50 K)	α (>100 K)	n (300 K) (10^{21} cm^{-3})	μ (300 K) (cm^2 V^{-1} S^{-1})	ΔE ($\times 10^{-7}$ eV)
$Ti_{0.07}TiS_2$	0.6836	2.04	3.23	1.56	1.32	3.40	7.6 ± 0.4
$Ti_{0.04}TiS_2$	0.2635	2.16	3.11	1.52	2.51	4.37	6.9 ± 0.1
$Ti_{0.02}TiS_2$	0.1482	3.05	2.90	1.41	1.98	6.96	2.1 ± 1.4
$Ti_{0.02}TiS_{2-x}O_x$	0.1997	6.01	2.57	1.90	0.40	13.12	12.5 ± 0.1

TiS_2 is beyond the scope of current work, but warrants further investigations.

In summary, the change of chemical compositions as well as the corresponding transport properties of defective TiS_2 were studied by using a combination of PES, Raman spectroscopy, and transport measurements. A low temperature resistivity upturn behavior demonstrates that TiS_2 is a heavily self-doped semiconductor with the Fermi level close to the CB, which can serve as conclusive experimental evidence regarding the semiconductor nature of TiS_2.[23] It is found that the electrical transport properties of TiS_2 are sensitive to the defects of Ti_i, Ti_F, and Ti–O species composed in TiS_2. (i) The high carrier concentration is attributed to the presence of Ti_i, which donates electrons to the conduction band of TiS_2. (ii) Ti_F leads to the localization of electrons, which is responsible for the reduction of the carrier concentration and electrical conductivity. (iii) High conductivity maintains upon partial oxidization, indicating high oxidization-tolerance in terms of the electronic structure. Our results suggest that the electrical transport properties of TiS_2 can be modulated by defect engineering, offering a new perspective for improving the performance of TiS_2-based devices.

See the supplementary material for the experimental details, Ti 2*p* and S 2*p* (measured by 600 eV), and valence band (measured by 100 eV) for $Ti_{0.02}TiS_2$ and $Ti_{0.02}TiS_{2-x}O_x$, peak fitting parameters extracted from the PES spectra, a log–log plot of $\rho_{xx}(T)$-ρ_0 vs T and power law fitting curves, and magnetic field dependence of ρ_{xx} and the Hall resistivity ρ_{xy}.

AUTHOR'S CONTRIBUTION

K.C. and M.S. contributed equally to this work.

This work was supported by the National Key Research and Development Program of China (Grant Nos. 2016YFA0300404, 2017YFA0402900, 2017YFA0403402, and 2017YFA0403403), the National Natural Science Foundation of China (NSFC) (Grant Nos. 11474288, 11574317, 11774341, 11774365, U1732272, 21872131, 11874358, and 11604344), and the Collaborative Innovation Program of Hefei Science Center, CAS. D.Q. acknowledges the support of the Australian Research Council (Grant No. FT160100207) and the continued support from the Queensland University of Technology (QUT) through the Centre for Materials Science. H.X. is thankful for the support of the Hundred Talents Program of the Chinese Academy of Sciences. The authors thank the BL11U beamline of the National Synchrotron Radiation Laboratory (NSRL) for providing the beam time. A portion of this work was supported by the High Magnetic Field Laboratory of Anhui Province.

The data that supports the finding of this study are available within the article and its supplementary material.

REFERENCES

[1]S. Das, A. Prakash, R. Salazar, and J. Appenzeller, ACS Nano **8**, 1681–1689 (2014).
[2]S.-H. Chung, L. Luo, and A. Manthiram, ACS Energy Lett. **3**, 568–573 (2018).
[3]E. Pomerantseva and Y. Gogotsi, Nat. Energy **2**, 17089 (2017).
[4]B. Tian, W. Tang, K. Leng, Z. Chen, S. J. R. Tan, C. Peng, G.-H. Ning, W. Fu, C. Su, G. W. Zheng, and K. P. Loh, ACS Energy Lett. **2**, 1835–1840 (2017).
[5]A. Chaturvedi, P. Hu, V. Aravindan, C. Kloc, and S. Madhavi, J. Mater. Chem. A **5**, 9177 (2017).
[6]C. Yin, Q. Hu, G. Wang, T. Huang, X. Zhou, X. Zhang, Y. Dou, B. Kang, J. Tang, N. Liu, and R. Ang, Appl. Phys. Lett. **110**, 043507 (2017).
[7]C. Wan, X. Gu, F. Dang, T. Itoh, Y. Wang, H. Sasaki, M. Kondo, K. Koga, K. Yabuki, G. J. Snyder, R. Yang, and K. Koumoto, Nat. Mater. **14**, 622–627 (2015).
[8]X. Huang, J. Tang, B. Luo, R. Knibbe, T. Lin, H. Hu, M. Rana, Y. Hu, X. Zhu, Q. Gu, D. Wang, and L. Wang, Adv. Energy Mater. **9**, 1901872 (2019).
[9]Y. Liu, C. Liang, J. Wu, T. Sharifi, H. Xu, Y. Nakanishi, Y. Yang, C. F. Woellne, A. Aliyan, A. A. Martí, B. Xie, R. Vajtai, W. Yang, and P. M. Ajayan, Adv. Mater. Interfaces **5**, 1700895 (2018).
[10]C. Lin, X. Zhu, J. Feng, C. Wu, S. Hu, J. Peng, Y. Guo, L. Peng, J. Zhao, J. Huang, J. Yang, and Y. Xie, J. Am. Chem. Soc. **135**, 5144–5151 (2013).
[11]H. Tao, M. Zhou, R. Wang, K. Wang, S. Cheng, and K. Jiang, Adv. Sci. **5**, 1801021 (2018).
[12]M. Zhang, C. Zhang, Y. You, H. Xie, H. Chi, Y. Sun, W. Liu, X. Su, Y. Yan, X. Tang, and C. Uher, ACS Appl. Mater. Interfaces **10**, 32344–32354 (2018).
[13]Z. Zeng, C. Tan, X. Huang, S. Bao, and H. Zhang, Energy Environ. Sci. **7**, 797–803 (2014).
[14]J.-H. Liao, Y.-C. Zhao, Y.-J. Zhao, X.-B. Yang, and Y. Chen, J. Appl. Phys. **127**, 044301 (2020).
[15]M. Beaumale, T. Barbier, Y. Bréard, G. Guelou, A. V. Powell, P. Vaqueiro, and E. Guilmeau, Acta Mater. **78**, 86–92 (2014).
[16]A. Samanta, T. Pandey, and A. K. Singh, Phys. Rev. B **90**, 174301 (2014).
[17]E. Guilmeau, T. Barbier, A. Maignan, and D. Chateigner, Appl. Phys. Lett. **111**, 133903 (2017).
[18]X. Sun, P. Bonnick, and L. F. Nazar, ACS Energy Lett. **1**, 297–301 (2016).
[19]C. Wan, Y. Kodama, M. Kondo, R. Sasai, X. Qian, X. Gu, K. Koga, K. Yabuki, R. Yang, and K. Koumoto, Nano Lett. **15**, 6302–6308 (2015).
[20]A. H. Thompson, F. R. Gamble, and C. R. Symon, Mater. Res. Bull. **10**, 915–919 (1975).
[21]J. A. Wilson, Phys. Status. Solidi B **86**, 11–36 (1978).
[22]A. Stoliaroff, C. Latouche, and S. Jobic, Phys. Rev. B **99**, 165122 (2019).
[23]H. Wang, Z. Qiu, W. Xia, C. Ming, Y. Han, L. Cao, J. Lu, P. Zhang, S. Zhang, H. Xu, and Y.-Y. Sun, J. Phys. Chem. Lett. **10**, 6996–7001 (2019).
[24]A. Stoliaroff, S. Jobic, and C. Latouche, Inorg. Chem. **58**, 1949–1957 (2019).
[25]G. Li, K. Yao, and G. Gao, Nanotechnology **29**, 015204 (2018).
[26]C. S. Cucinotta, K. Dolui, H. Pettersson, Q. M. Ramasse, E. Long, S. E. O'Brian, V. Nicolosi, and S. Sanvito, J. Phys. Chem. C **119**, 15707–15715 (2015).
[27]C. A. Kukkonen, W. J. Kaiser, E. M. Logothetis, B. J. Blumenstock, P. A. Schroeder, S. P. Faile, R. Colella, and J. Gambold, Phys. Rev. B **24**, 1691 (1981).
[28]D. Y. Oh, Y. E. Choi, D. H. Kim, Y.-G. Lee, B.-S. Kim, J. Park, H. Sohn, and Y. S. Jung, J. Mater. Chem. A **4**, 10329 (2016).
[29]H. Martinez, C. Auriel, D. Gonbeau, M. Loudet, and G. Pfister-Guillouzo, Appl. Surf. Sci. **93**, 231–235 (1996).
[30]L. Cao, Y. Wang, J. Zhong, Y. Han, W. Zhang, X. Yu, F. Xu, D.-C. Qi, and A. T. S. Wee, J. Phys. Chem. C **115**, 24880–24887 (2011).
[31]S. Okeil, S. Yadav, M. Bruns, A. Zintler, L. Molina-Luna, and J. J. Schneider, Dalton Trans. **49**, 1032–1047 (2020).
[32]M. P. Seah, I. S. Gilmore, and S. J. Spencer, J. Electron. Spectrosc. Relat. Phenom. **120**, 93–111 (2001).
[33]P. C. Sherrell, K. Sharda, C. Grotta, J. Ranalli, M. S. Sokolikova, F. M. Pesci, P. Palczynski, V. L. Bemmer, and C. Mattevi, ACS Omega **3**, 8655–8662 (2018).
[34]B. Choudhury and A. Choudhury, J. Appl. Phys. **114**, 203906 (2013).
[35]B. Liu, J. Yang, Y. Han, T. Hu, W. Ren, C. Liu, Y. Ma, and C. Gao, J. Appl. Phys. **109**, 053717 (2011).
[36]A. H. Thompson, Phys. Rev. Lett. **35**, 1786 (1975).
[37]D. Suri, V. Siva, S. Joshi, K. Senapati, P. K. Sahoo, S. Varma, and R. S. Patel, J. Phys.: Condens. Matter **29**, 485708 (2017).
[38]J. M. Moya, C.-L. Huang, J. Choe, G. Costin, M. S. Foster, and E. Morosan, Phys. Rev. Mater. **3**, 084005 (2019).
[39]S. Barua, M. C. Hatnean, M. R. Lees, and G. Balakrishnan, Sci. Rep. **7**, 10964 (2017).
[40]P. C. Klipstein, A. G. Bagnall, W. Y. Liang, E. A. Marseglia, and R. H. Friend, J. Phys. C **14**, 4067 (1981).
[41]W. Yuan, L. Cheng, Y. An, S. Lv, H. Wu, X. Fan, Y. Zhang, X. Guo, and J. Tang, Adv. Sci. **5**, 1700870 (2018).
[42]Z. Hu, Z. Tai, Q. Liu, S.-W. Wang, H. Jin, S. Wang, W. Lai, M. Chen, L. Li, L. Chen, Z. Tao, and S.-L. Chou, Adv. Energy Mater. **9**, 1803210 (2019).
[43]Y.-S. Hu, L. Kienle, Y.-G. Guo, and J. Maier, Adv. Mater. **18**, 1421–1426 (2006).